Title

Dosimetric impact from cardiac motion to heart substructures in thoracic cancer patients treated with a magnetic resonance guided radiotherapy system.

Authors

Chu, Fang-I
Gao, Yu
Yu, Victoria
et al.

Publication Date

2021

DOI

10.1016/j.phro.2020.11.005

Peer reviewed

Physics and Imaging in Radiation Oncology 17 (2021) 8–12

Contents lists available at ScienceDirect

Physics and Imaging in Radiation Oncology

journal homepage: www.sciencedirect.com/journal/physics-and-imaging-in-radiation-oncology

Technical Note

Dosimetric impact from cardiac motion to heart substructures in thoracic cancer patients treated with a magnetic resonance guided radiotherapy system

Ran Yan [a,b], Fang-I Chu [c], Yu Gao [a], Victoria Yu [a,1], Stephanie Yoon [c], David Elashoff [d], Percy Lee [e], Peng Hu [a], Yingli Yang [c,*]

[a] Department of Radiological Sciences, David Geffen School of Medicine, University of California, Los Angeles, CA, USA
[b] Department of Bioengineering, University of California, Los Angeles, CA, USA
[c] Department of Radiation Oncology, University of California, Los Angeles, CA, USA
[d] Department of Biostatistics, University of California, Los Angeles, CA, USA
[e] Department of Radiation Oncology, MD Anderson Cancer Center, Houston, TX, USA

ARTICLE INFO

Keywords:
Dosimetry analysis
Cardiac substructures
CINE MRI
MRgRT

ABSTRACT

Few studies have examined the cardiac volume and radiation dose differences among cardiac phases during radiation therapy (RT). Such information is crucial to dose reconstruction and understanding of RT related cardiac toxicity. In a cohort of nine patients, we studied the changes in the volume and doses of several cardiac substructures between the end-diastolic and end-systolic phases based on the clinical magnetic resonance-guided RT (MRgRT) treatment plans. Significant differences in the volume and dose between the two phases were observed. Onboard cardiac cine MRI holds promise for patient-specific cardiac sparing treatment designs.

1. Introduction

Substantial radiation dose to the heart during radiation therapy (RT) is associated with an increased risk of cardiac toxicity and worse overall survival [1,2]. Radiation doses received by the heart from thoracic RT for lymphoma, lung, breast, and esophageal cancers can be substantial and consequential for long-term cardiac health [3–6]. Cardiac substructures, including the ventricles, the atria, the valves, and the great arteries, all contribute to cardiac function. Several studies have demonstrated a strong relationship between radiation doses to these substructures or cardiac subregions and the risk for developing cardiac disease [7–11].

Multiple studies measured the magnitude of the cardio-respiratory motion of the heart and its substructures among free-breathing patients [12,13]. However, deep inhalation breath-hold (DIBH) represents one of the most well studied cardiac sparing techniques [14], and its application leads to the necessity of accurate information about the substructure motion and dose variation due to cardiac activity. The extent of displacements of the left ventricle and coronary arteries arising from intrinsic cardiac contraction has previously been evaluated using cardiac-gated CT and MRI [15–17]. However, there were limited studies analyzing the dose-volume parameter variation for these cardiac substructures in a time-resolved manner during a cardiac cycle, which is the main focus of this study. Such dynamic information may be crucial for accurately calculating cardiac dose and a better understanding of RT related cardiac toxicity. MRI-guided radiation therapy (MRgRT), with its onboard MRI, offers the option of acquiring cardiac MR images while the patient is in RT treatment position [18] and time-resolved cardiac doses. The potential incorporation of time-resolved cardiac substructure dose-volume information into the MRgRT treatment sessions may offer an opportunity to reduce RT-related cardiac toxicity by optimizing the timing of beam delivers to minimize RT dose.

In this study, we aimed to evaluate radiation doses to various cardiac substructures at end-diastolic and end-systolic cardiac phases based on cardiac cine MRI. We hypothesized that variation in cardiac substructure shape and position during RT delivery due to cardiac activity would significantly impact the dose delivered to the cardiac substructures.

* Corresponding author at: 200 UCLA Medical Plaza Suite B265, Los Angeles, CA 90095, USA.
E-mail address: yyang@mednet.ucla.edu (Y. Yang).
[1] Present address: Department of Medical Physics, Memorial Sloan Kettering Cancer Center, New York, NY, USA.

https://doi.org/10.1016/j.phro.2020.11.005
Received 15 June 2020; Received in revised form 24 November 2020; Accepted 25 November 2020
Available online 18 December 2020

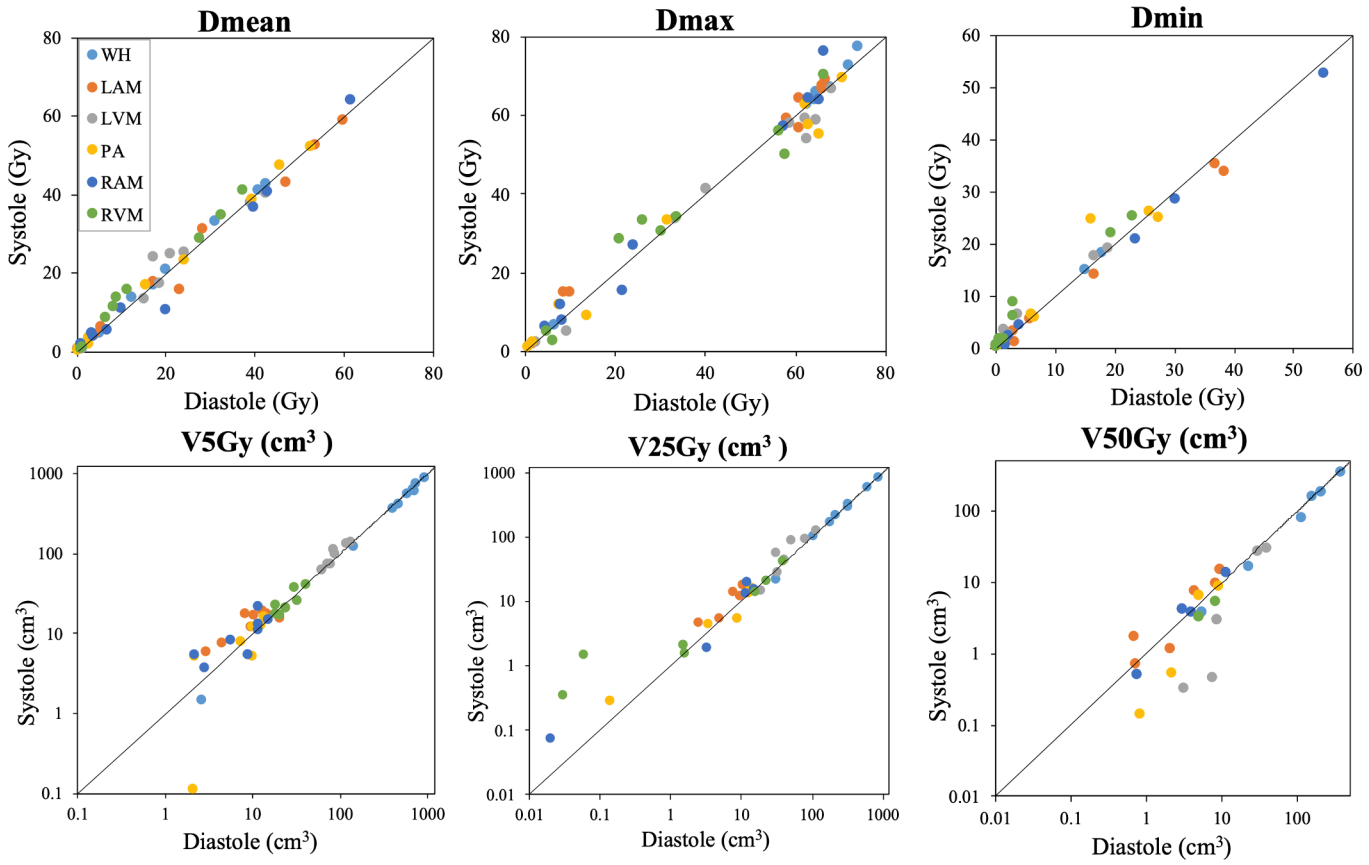

Fig. 1. Dose metrics comparison between diastolic and systolic phases for whole-heart and five cardiac substructures. The volume metrics are displayed on a logarithmic scale due to the broad range of values. WH: whole heart; LVM: left ventricle myocardium; RVM: right ventricle myocardium; RAM: right atrium myocardium; LAM: left atrium myocardium; PA: pulmonary artery.

2. Materials and methods

2.1. Cardiac MRI protocol

Our patient study was conducted using a 0.35T MRgRT system (ViewRay, Mountain View, CA) under a protocol approved by our institutional review board. Each patient signed an informed consent before the study. Nine patients with centrally located thoracic tumors who underwent clinical RT treatment using our MRgRT system were recruited between 2017 and 2018 (five males and four females, age: 60 ± 17 years). For each patient, an ECG-gated multi-slice balanced Steady-State Free Precession (bSSFP) cine MRI sequence was used to perform whole-heart imaging using the onboard MRI. Multiple axial slices during repeated breath-holds were acquired to cover the whole heart from the aortic arch to the apex. During each image acquisition, the patient performed nine breath-holds. For each breath-hold, three slices of images with multiple cardiac phases were acquired. The DIBH technique was used to minimize respiratory motion. The imaging parameters were as follows: TR/TE = 4/2 ms, slice thickness = 7 mm, matrix 256x192x25, the field of view = 361x270mm^2, flip angle = 130°, bandwidth = 720 Hz/pixel, 12 cardiac phases, parallel imaging using the GeneRalized Autocalibrating Partial Parallel Acquisition (GRAPPA) approach with an acceleration factor of two [19].

2.2. Radiation dose calculation

Disease sites, prescription doses, and tumor characteristics were summarized in Supplementary Table 1. Based on the CINE MRI, the whole heart (WH) and five cardiac substructures (right ventricle myocardium (RVM), left ventricle myocardium (LVM), right atrium myocardium (RAM), left atrium myocardium (LAM) and pulmonary artery vessel wall (PA)) were contoured separately for the end-systolic and end-diastolic phases by a radiation oncologist. The cavities of the four cardiac chambers and pulmonary artery were not included in the contours. The cardiac substructure delineation and dose metrics extraction were performed using commercial software (MIM Software Inc., Cleveland, OH). Patient planning CT was deformably registered to the corresponding end-diastolic and end-systolic images from the CINE MRI data separately. Subsequently, electron density was transferred from CT to the deformably co-registered MR images for forward dose calculations. The dose maps were slightly different between the two cardiac phases due to the difference in the beam pathways caused by the different anatomy. The treatment planning system (TPS) used to perform dose calculations was the MRIdian Treatment Planning and Delivery Software (TPDS) (MRIdian, ViewRay Inc., Oakwood Village, OH). The following dose metrics were collected for the cardiac structures: mean dose (Dmean), maximum dose (Dmax) and minimum dose (Dmin) in Gy, and volume receiving 5 Gy (V5Gy), 25 Gy (V25Gy), and 50 Gy (V50Gy) in cm^3.

2.3. Evaluation of differences in volume and doses

The volume variation of cardiac structure between the two cardiac phases was analyzed. Hausdorff distance (HD) [20] and Dice similarity coefficient (DSC) [21] were used to measure the distance and spatial overlap of cardiac structure contours, assuming DSC = 0.7 as the cut-off for fairly good overlap [22]. The dose-volume parameters of the end-diastolic and end-systolic phases were analyzed and compared. The mean absolute difference and the rate of variation of the dose metrics were calculated. Dose-volume parameter differences that were normally

Table 1
Dose-volume parameters variation for WH, LAM, LVM, PA, RAM, and RVM between the end-diastolic and end-systolic phases and adjusted P-value of the two-sided paired *t*-test.

Dose Metrics	Absolute Difference Mean (SD)	Rate of change (%) Mean (SD)	P-value	Dose Metrics	Absolute Difference Mean (SD)	Rate of change (%) Mean (SD)	P-value
WH							
Dmean (Gy)	0.6 (0.6)	4.6 (4.0)	0.45	V5Gy (cm^3)	55.7 (37.5)	15.6 (12.60)	**0.01**
Dmax (Gy)	0.8 (0.9)	1.3 (1.1)	0.36	V25Gy (cm^3)	25.1 (25.3)	11.0 (9.4)	**0.11**
Dmin (Gy)	0.1 (0.1)	6.5 (7.1)	0.61	V50Gy (cm^3)	11.0 (14.5)	18.5 (13.1)	**0.15**
LAM							
Dmean (Gy)	2.0 (2.4)	8.5 (9.5)	0.45	V5Gy (cm^3)	4.1 (2.8)	32.7 (13.4)	0.23
Dmax (Gy)	2.6 (2.0)	11.4 (14.8)	0.36	V25Gy (cm^3)	2.2 (2.5)	31.4 (14.7)	0.42
Dmin (Gy)	1.4 (1.7)	19.6 (23.6)	**0.11**	V50Gy (cm^3)	1.2 (1.7)	32.3 (21.4)	0.25
LVM							
Dmean (Gy)	2.1 (2.0)	14.6 (15.9)	0.78	V5Gy (cm^3)	5.9 (7.1)	18.9 (33.3)	0.5
Dmax (Gy)	3.0 (3.0)	10.8 (15.3)	**0.19**	V25Gy (cm^3)	9.0 (12.2)	20.2 (17.1)	0.42
Dmin (Gy)	0.6 (0.9)	17.1 (18.9)	**0.13**	V50Gy (cm^3)	3.4 (4.1)	58.2 (36.5)	**0.15**
PA							
Dmean (Gy)	0.8 (0.5)	10.4 (13.2)	0.78	V5Gy (cm^3)	1.6 (1.7)	32.9 (35.2)	0.90
Dmax (Gy)	3.1 (3.5)	12.0 (13.9)	0.36	V25Gy (cm^3)	0.8 (1.3)	25.2 (20.5)	0.79
Dmin (Gy)	1.4 (2.8)	14.1 (15.5)	0.61	V50Gy (cm^3)	0.5 (0.7)	46.4 (38.9)	0.57
RAM							
Dmean (Gy)	2.4 (2.9)	15.8 (14.9)	0.45	V5Gy (cm^3)	2.6 (2.9)	35.2 (30.7)	0.50
Dmax (Gy)	3.1 (3.1)	13.3 (12.4)	0.63	V25Gy (cm^3)	1.2 (2.3)	39.2 (38.3)	0.61
Dmin (Gy)	1.0 (1.2)	13.3 (20.4)	**0.12**	V50Gy (cm^3)	0.3 (0.6)	18.8 (13.6)	0.32
RVM							
Dmean (Gy)	2.4 (1.6)	21.8 (13.2)	**0.06**	V5Gy (cm^3)	3.5 (2.6)	26.4 (30.4)	0.51
Dmax (Gy)	3.4 (3.4)	14.0 (19.2)	0.71	V25Gy (cm^3)	0.9 (1.1)	36.6 (42.3)	0.69
Dmin (Gy)	1.6 (1.9)	27.4 (21.7)	**0.11**	V50Gy (cm^3)	0.6 (1.1)	57.9 (36.4)	0.25

The numbers in bold indicate significant dose differences between the two cardiac phases with adjusted P-values. WH: whole heart; LVM: left ventricle myocardium; RVM: right ventricle myocardium; RAM: right atrium myocardium; LAM: left atrium myocardium; PA: pulmonary artery. Dmean: mean dose; Dmax: maximum dose; Dmin: minimun dose; V5Gy: volume receiving 5 Gy; V25Gy: volume receiving 25 Gy; V50Gy: volume receiving 50 Gy.

distributed were assessed via a two-sided paired *t*-test. With the explorative aim, the false discovery rate (FDR) was controlled via the Benjamini-Hochberg procedure [23] to accommodate multiple testing issues with a threshold level for adjusted P-values of 0.2 [24,25]. The intra-class correlation coefficient (ICC) was then used to assess the consistency of dose difference between two phases among cardiac structures and patients [26].

3. Results

Volume variation, Hausdorff distances, and DSCs of cardiac structures between the two cardiac phases are shown in Supplementary Table 2. The volumes of the WH, LVM, and RVM were decreased in end-systole by a mean volume difference of 99.5 cm^3, 2.8 cm^3, 6.8 cm^3. However, the volumes of the LAM, RAM, and PA were increased in end-systole by a mean volume difference of 3.9 cm^3, 3.7 cm^3, and 0.2 cm^3. The mean Hausdorff distance variations were <20 mm for the WH, LAM, LVM, and PA and >20 mm for RAM and RVM. For all patients, the DSCs were >0.7 for the WH and <0.7 for the other cardiac substructures. Supplementary Fig. 1 shows an example of cardiac structure contours in MRIs and dose maps of end-diastolic and end-systolic phases. Volumetric and morphological changes of the cardiac substructures were observed. Differences in the dose maps could also be seen. The dose-volume histogram of the same patient is shown in Supplementary Fig. 2. For this patient, the doses to the LVM, RAM, LAM were increased in end-diastole, whereas the doses to the RVM and PA were increased in end-systole.

Dose variations to the WH and cardiac substructures between end-diastolic and end-systolic phases are illustrated in Fig. 1 and Supplementary Fig. 3, and summarized in Table 1. According to Fig. 1, a tendency of variation in the dose-volume difference was observed. Significant dose-volume differences between the two cardiac phases (adjusted $P < 0.2$) were observed for: V5Gy, V25Gy and V50Gy to the WH; Dmax, Dmin and V50Gy to the LVM; Dmean and Dmin to the RVM; Dmin to the LAM; and Dmin to the RAM. No dose metrics to the PA were found to be significantly different (Table 1). The absolute differences of Dmean, Dmax, and Dmin to the WH were lower than other cardiac substructures, whereas these differences to the RVM were higher than other cardiac structures. The absolute differences of Dmax were the highest among dose parameters for all cardiac structures. The rates of change of V5Gy, V25Gy, and V50Gy to all of the cardiac structures were $> 10\%$. The rates of change of all dose-volume parameters to the WH were lower than other cardiac substructures (for additional details, see

Supplementary Table 3).

The intra-class correlation coefficients of all dose-volume differences between the two cardiac phases among all substructures and patients were less than 0.75, indicating a low to moderate consistency.

4. Discussion

This study evaluated the whole-heart and cardiac substructure dose-volume differences between the end-diastolic and end-systolic phases. We found significant dose-volume differences to the WH, LVM, and RVM. To the best of our knowledge, this is the first study comparing cardiac substructure volume and radiation doses among different cardiac phases during breath holds using onboard MRI of an MRgRT system.

A study by Bahig et al. [27] evaluated the radiation dose variation to the WH and LV (including blood pool) during the cardiac cycle for patients with left-sided breast cancer using dual source computed tomography (DSCT). They found that the WH Dmax and V5Gy were decreased in systole, and Dmax to the LV was lower in systole, consistent with our findings. Likewise, Tong et al. [28] assessed the variation in dose-volume parameters to the WH and LVM caused by cardiac activity for the patients with thoracic esophageal carcinomas using 4DCT. They found a significant difference in Dmean, V5Gy, V10Gy, V20Gy, V30Gy, and V40Gy for the LVM. In our study, a detailed analysis was performed on a larger number of cardiac substructures and their dose-volume parameters, giving more comparisons with significant differences compared to prior studies. More importantly, we used cardiac bSSFP cine MRIs for cardiac substructure contouring, which provided superior soft-tissue contrast as compared with prior studies utilizing CT. One other major difference and merit of our study is that by excluding the blood pool in the cardiac chambers and pulmonary arteries from contours, all dosimetric analyses were performed solely on the cardiac tissue relevant to the development of cardiac side effects.

In this study, we found the most significant dose difference was observed for the WH, RVM, and LVM. This was related to the sizeable physiological variation in positions, sizes, and shapes of these three structures during the cardiac cycle. For the RAM, LAM, and PA, although the DSCs were significantly lower than 0.7, there were less significant dose differences, which might be because the position and shape changes over cardiac phases of the myocardium of the atria and pulmonary artery wall were quantitatively small but significant relative to their size. As shown in Supplementary Fig. 3, we could not reach a general conclusion regarding which phase provided better cardiac sparing for all substructions. For example, for LVM, Dmin had a higher value at the end-systolic phase, while Dmax and V50Gy had a higher value at the end-diastolic phase.

The intra-fraction motion of tumors observed from cine MRI during radiation therapy for different disease sites has been investigated in multiple studies [29–31]. However, the intra-fraction motion of the heart during radiation therapy, especially cardiac substructures, might be a non-trivial but overlooked source of treatment error. Our study showed the value of considering cardiac motion when evaluating cardiac RT toxicity. The value of paying attention to cardiac substructures during RT has been shown in different studies [5,10,32,33]. Being able to correlate toxicity with the actual dose received by each substructure will further our understanding of the mechanism of radiation toxicity to the heart and provide guidance on cardiac sparing treatment.

This study has a few limitations. The patient cohort size is relatively small. While our analysis and data acquisition with the limited subjects show novelty and great promise, a more comprehensive study with a larger patient cohort is needed to strengthen conclusions further. Also, other cardiac substructures that could potentially relate to certain cardiovascular diseases (CVDs), such as coronary artery and valves, were not yet investigated. In addition, only the two extreme cardiac phases were investigated without considering phases in between. As part of future work, cardiac dose reconstruction accuracy could be further improved by incorporating the whole cardiac cycle. Lastly, due to the acquisitions spanning over multiple breath-holds, the variation between breath-hold positions could result in slice misalignment. However, only two of the nine patients' images showed minor discontinuities in the slice direction.

In conclusion, there were significant differences in volume and dose for cardiac substructures between the two cardiac phases we studied. Cardiac cine MRI would be crucial for accurate cardiac dose reconstruction if incorporated into post-treatment evaluation. It might also hold promises for patient-specific cardiac sparing treatment design to improve treatment efficacy.

Declaration of Competing Interest

The authors declare that they have no known competing financial interests or personal relationships that could have appeared to influence the work reported in this paper.

Acknowledgements

This paper is part of a special issue that contains contributions originally submitted to the scientific meeting MR in RT, which was planned to take place 05/2020, organized by the German Research Center (DKFZ) in Heidelberg. We acknowledge funding by DKFZ for the publication costs of this special issue.

Appendix A. Supplementary data

Supplementary data to this article can be found online at https://doi.org/10.1016/j.phro.2020.11.005.

References

[1] Bradley JD, Paulus R, Komaki R, Masters G, Blumenschein G, Schild S, et al. Standard-dose versus high-dose conformal radiotherapy with concurrent and consolidation carboplatin plus paclitaxel with or without cetuximab for patients with stage IIIA or IIIB non-small-cell lung cancer (RTOG 0617): a randomised, two-by-two factorial p. Lancet Oncol 2015;16:187–99. https://doi.org/10.1016/S1470-2045(14)71207-0.

[2] Speirs CK, DeWees TA, Rehman S, Molotievschi A, Velez MA, Mullen D, et al. Heart dose is an independent dosimetric predictor of overall survival in locally advanced non–small cell lung cancer. J Thoracic Oncol 2017;12(2):293–301. https://doi.org/10.1016/j.jtho.2016.09.134.

[3] van Nimwegen FA, Schaapveld M, Cutter DJ, Janus CPM, Krol ADG, Hauptmann M, et al. Radiation dose-response relationship for risk of coronary heart disease in survivors of hodgkin lymphoma. J Clin Oncol 2016;34(3):235–43. https://doi.org/10.1200/JCO.2015.63.4444.

[4] Wang K, Eblan MJ, Deal AM, Lipner M, Zagar TM, Wang Y, et al. Cardiac toxicity after radiotherapy for stage III non–small-cell lung cancer: pooled analysis of dose-escalation trials delivering 70 to 90 Gy. JCO 2017;35(13):1387–94. https://doi.org/10.1200/JCO.2016.70.0229.

[5] Piroth MD, Baumann R, Budach W, Dunst J, Feyer P, Fietkau R, et al. Heart toxicity from breast cancer radiotherapy: current findings, assessment, and preventionKardiale Toxizität durch Strahlentherapie bei Brustkrebs: Aktuelle Ergebnisse, Bewertung und Prävention. Strahlenther Onkol 2019;195(1):1–12. https://doi.org/10.1007/s00066-018-1378-z.

[6] Beukema JC, van Luijk P, Widder J, Langendijk JA, Muijs CT. Is cardiac toxicity a relevant issue in the radiation treatment of esophageal cancer? Radiother Oncol 2015;114(1):85–90. https://doi.org/10.1016/j.radonc.2014.11.037.

[7] Ma J-T, Sun Li, Sun X, Xiong Z-C, Liu Y, Zhang S-L, et al. Is pulmonary artery a dose-limiting organ at risk in non-small cell lung cancer patients treated with definitive radiotherapy? Radiat Oncol 2017;12(1). https://doi.org/10.1186/s13014-017-0772-5.

[8] Stam B, Peulen H, Guckenberger M, Mantel F, Hope A, Werner-Wasik M, et al. Dose to heart substructures is associated with non-cancer death after SBRT in stage I–II NSCLC patients. Radiother Oncol 2017;123(3):370–5. https://doi.org/10.1016/j.radonc.2017.04.017.

[9] Hahn E, Jiang H, Ng A, Bashir S, Ahmed S, Tsang R, et al. Late cardiac toxicity after mediastinal radiation therapy for hodgkin lymphoma: contributions of coronary artery and whole heart dose-volume variables to risk prediction. Int J Radiat Oncol*Biol*Phys 2017;98(5):1116–23. https://doi.org/10.1016/j.ijrobp.2017.03.026.

[10] van den Bogaard VAB, Ta BDP, van der Schaaf A, Bouma AB, Middag AMH, Bantema-Joppe EJ, et al. Validation and modification of a prediction model for acute cardiac events in patients with breast cancer treated with radiotherapy based

on three-dimensional dose distributions to cardiac substructures. J Clin Oncol 2017;35(11):1171–8. https://doi.org/10.1200/JCO.2016.69.8480.
[11] McWilliam A, Dootson C, Graham L, Banfill K, Abravan A, van Herk M. Dose surface maps of the heart can identify regions associated with worse survival for lung cancer patients treated with radiotherapy. Phys Imaging Radiat Oncol 2020; 15:46–51. https://doi.org/10.1016/j.phro.2020.07.002.
[12] Guzhva L, Flampouri S, Mendenhall NP, Morris CG, Hoppe BS. Intrafractional displacement of cardiac substructures among patients with mediastinal lymphoma or lung cancer. Adv Radiat Oncol 2019;4(3):500–6. https://doi.org/10.1016/j.adro.2019.03.008.
[13] Vasquez Osorio EM, McCallum H, Bedair A, Faivre-Finn C, Haughey A, van Herk M, et al. Protecting the heart: a practical approach to account for the full extent of heart motion in radiation therapy planning. Int J Radiat Oncol*Biol*Phys 2020; 108(4):1082–90. https://doi.org/10.1016/j.ijrobp.2020.06.068.
[14] Ledsom D, Reilly AJ, Probst H. Assessment of deep inspiration breath hold (DIBH) amplitude and reduction in cardiac dose in left breast cancer patients. Radiography 2018;24(2):98–103. https://doi.org/10.1016/j.radi.2017.11.005.
[15] Kataria T, Bisht SS, Gupta D, Abhishek A, Basu T, Narang K, et al. Quantification of coronary artery motion and internal risk volume from ECG gated radiotherapy planning scans. Radiother Oncol 2016;121(1):59–63. https://doi.org/10.1016/j.radonc.2016.08.006.
[16] Tong Y, Yin Y, Lu J, Liu T, Chen J, Cheng P, et al. Quantification of heart, pericardium, and left ventricular myocardium movements during the cardiac cycle for thoracic tumor radiotherapy. Onco Targets Ther 2018;11:547–54. https://doi.org/10.2147/OTT.S155680.
[17] Levis M, De Luca V, Fiandra C, Veglia S, Fava A, Gatti M, et al. Plan optimization for mediastinal radiotherapy: estimation of coronary arteries motion with ECG-gated cardiac imaging and creation of compensatory expansion margins. Radiother Oncol 2018;127(3):481–6. https://doi.org/10.1016/j.radonc.2018.04.014.
[18] Rashid S, Han F, Gao Y, Sung K, Cao M, Yang Y, et al. Cardiac balanced steady-state free precession MRI at 0.35 T: a comparison study with 1.5 T. Quant. Imaging Med. Surg. 2018;8(7):627–36. https://doi.org/10.21037/qims.2018.08.09.
[19] Griswold MA, Jakob PM, Heidemann RM, Nittka M, Jellus V, Wang J, Kiefer B, Haase A. Generalized autocalibrating partially parallel acquisitions (GRAPPA). Magn. Reson. Med. 2002;47(6):1202–10. https://doi.org/10.1002/mrm.10171.
[20] Huttenlocher DP, Klanderman GA, Rucklidge WJ. Comparing Images Using the Hausdorff Distance. IEEE Trans Pattern Anal Mach Intell 1993;15:850–63. doi: 10.1109/34.232073.
[21] Dice LR. Measures of the amount of ecologic association between species. Ecology 1945;26:297–302. doi: 10.2307/1932409.
[22] Robinson R, Valindria VV, Bai W, Oktay O, Kainz B, Suzuki H, et al. Automated quality control in image segmentation: application to the UK Biobank cardiovascular magnetic resonance imaging study. J Cardiovasc Magn Reson 2019; 21(1). https://doi.org/10.1186/s12968-019-0523-x.
[23] Benjamini Y, Hochberg Y. Controlling the false discovery rate: a practical and powerful approach to multiple testing. J R Stat Soc Ser B 1995;57:289–300. doi: 10.1111/j.2517-6161.1995.tb02031.x.
[24] Capanu M, Seshan VE. False discovery rates for rare variants from sequenced data. Genet Epidemiol 2015;39:65–76. doi: 10.1002/gepi.21880.
[25] Amar D, Shamir R, Yekutieli D. Extracting replicable associations across multiple studies: Empirical Bayes algorithms for controlling the false discovery rate. PLoS Comput Biol 2017;13:e1005700. doi: 10.1371/journal.pcbi.1005700.
[26] Koo TK, Li MY. A guideline of selecting and reporting intraclass correlation coefficients for reliability research. J Chiropractic Med 2016;15(2):155–63. https://doi.org/10.1016/j.jcm.2016.02.012.
[27] Bahig H, de Guise J, Vu T, Blais D, Chartrand-Lefebvre C, Nguyen NT, et al. In a heartbeat: an assessment of dynamic dose variation to cardiac structures using dual source computed tomography. Int J Radiat Oncol*Biol*Phys 2018;102(4):950–9. https://doi.org/10.1016/j.ijrobp.2018.01.049.
[28] Tong Y, Yin Y, Cheng P, Lu J, Liu T, Chen J, et al. Quantification of variation in dose-volume parameters for the heart, pericardium and left ventricular myocardium during thoracic tumor radiotherapy. J Radiat Res 2018;59:462–8. doi: 10.1093/jrr/rry026.
[29] Bruijnen T, Stemkens B, Terhaard C, Lagendijk JJW, Raaijmakers CP, Tijssen RH. MRI-based radiation therapy: intrafraction motion quantification of head and neck tumors using cine magnetic resonance imaging. Int J Radiat Oncol*Biol*Phys 2018;100(5):1358. https://doi.org/10.1016/j.ijrobp.2017.12.134.
[30] Cusumano D, Dhont J, Boldrini L, Chiloiro G, Teodoli S, Massaccesi M, et al. Predicting tumour motion during the whole radiotherapy treatment: a systematic approach for thoracic and abdominal lesions based on real time MR. Radiother Oncol 2018;129(3):456–62. https://doi.org/10.1016/j.radonc.2018.07.025.
[31] Heethuis SE, Borggreve AS, Goense L, Van Rossum PSN, Mook S, Van Hillegersberg R, et al. Quantification of variations in intra-fraction motion of esophageal tumors over the course of neoadjuvant chemoradiotherapy based on cine-MRI. Phys Med Biol 2018;63:145019. doi: 10.1088/1361-6560/aacfb5.
[32] Jacob S, Camilleri J, Derreumaux S, Walker V, Lairez O, Lapeyre M, et al. Is mean heart dose a relevant surrogate parameter of left ventricle and coronary arteries exposure during breast cancer radiotherapy: a dosimetric evaluation based on individually-determined radiation dose (BACCARAT study). Radiat Oncol 2019;14 (1). https://doi.org/10.1186/s13014-019-1234-z.
[33] Hoppe BS, Bates JE, Mendenhall NP, Morris CG, Louis D, Ho MW, Hoppe RT, Shaikh M, Li Z, Flampouri S. The meaningless meaning of mean heart dose in mediastinal lymphoma in the modern radiation therapy era. Practical Radiat Oncol 2020;10(3):e147–54. https://doi.org/10.1016/j.prro.2019.09.015.